33. II–IV Semiconductors for Optoelectronics: CdS, CdSe, CdTe

Minoru Isshiki, Jifeng Wang

Owing to their suitable band gaps and high absorption coefficients, Cd-based compounds such as CdTe and CdS are the most promising photovoltaic materials available for low-cost high-efficiency solar cells. Additionally, because of their large atomic number, Cd-based compounds such as CdTe and CdZnTe, have been applied to radiation detectors. For these reasons, preparation techniques for these materials in the polycrystalline films and bulk single crystals demanded by these devices have advanced significantly in recent decades, and practical applications have been realized in optoelectronic devices. This chapter mainly describes the application of these materials in solar cells and radiation detectors and introduces recent progress.

33.1 Background

Cd-based compounds are very important semiconductor materials in the II–VI family. The attraction of Cd-based binary and ternary compounds arises from their promising applications as solar cells, γ- and x-ray detectors etc. These devices made from Cd-based materials are being widely applied in many fields.

33.2 Solar Cells

With the development of human society, energy sources in the earth are being slowly exhausted and we are faced with a serious problem. The solar cell is one substitute for fossil fuels and is being realized throughout the world. For this reason, solar-cell technologies have been developed since work was started by *Becquerel* in 1839 [33.1]. The solar cell has now been applied to daily life, industry, agriculture, space exploration, military affairs etc.

Solar cells have many advantages. Firstly, sunlight as an energy source for power generation is not only limitless but can be used freely. Secondly, since light is directly converted to electricity, the conversion process is clean, noise-free and not harmful to the environment, unlike a mechanical power generator. Thirdly, solar cells need little maintenance.

33.2.1 Basic Description of Solar Cells

A solar cell is a semiconductor device that directly converts light energy into electrical energy through the photovoltaic process. The basic structure of a solar cell is shown in Fig. 33.1. A typical solar cell consists of a junction formed between an n-type and a p-type semiconductor, of the same (homojunction) or different materials (heterojunction), an antireflection coating and Ohmic collecting electrodes. When the light irradiates the surface of a solar cell, photons with an energy

S. Kasap, P. Capper (Eds.), *Springer Handbook of Electronic and Photonic Materials*, DOI 10.1007/978-3-319-48933-9_33

greater than the band gap of the semiconductor are absorbed by the semiconductor material. This absorption activates electron transitions from the valence to the conduction band, so that electron–hole pairs are generated. If these carriers can diffuse into the depletion region before they recombine, they can be separated by the applied electric field. At the p–n junction, the negative electrons diffuse into the n-type region and the positive holes diffuse into the p-type region. They are then collected by electrodes, resulting in a voltage difference between the two electrodes. When an external load is connected, electric current flows through the load. This is the origin of the solar cell's photocurrent.

Three parameters can be used to describe the performance of a solar cell: the short-circuit current density (J_{SC}), the open-circuit voltage (V_{OC}) and the fill factor (FF).

The short-circuit current density J_{SC} is the photocurrent output from a solar cell when the output terminals are short-circuited. In the ideal case, this is equal to the current density generated by the light J_L and is proportional to the incident photon flux. J_{SC} is determined by the spectral response of the device, the junction depth, and the series (internal) resistance, R_s. The open-circuit voltage V_{OC} is the voltage appearing across the output terminals of the cell when there is no load present, i. e., when $J = 0$. The relationship between V_{OC} and J_{SC} can be described by the diode equation, i. e.,

$$V_{OC} = \frac{nk_BT}{e} \ln\left(\frac{J_{SC}}{J_0} + 1\right), \tag{33.1}$$

where e, n, J_0, k_B and T are the charge on an electron, the diode ideality factor, the reverse saturation-current density, the Boltzmann constant and the absolute temperature, respectively. The fill factor (FF) is the ratio of the maximum electrical power available from the cell (i. e., at the operating point J_m, V_m) in Fig. 33.2) to the product ofV_{OC} and J_{SC}. It describes the rectangularity of the photovoltaic output characteristic.

$$FF = \frac{V_mJ_m}{V_{oc}J_{sc}} = \frac{P_m}{V_{oc}J_{sc}}. \tag{33.2}$$

The conversion efficiency (η) of a solar cell is determined as

$$\eta = \frac{P_m}{P_s} = \frac{V_{oc}J_{sc}FF}{P_s}. \tag{33.3}$$

Where P_s is the incident illumination power and P_m is the output electricity power, both being per unit area. The relationship between the short-circuit current density J_{SC} and the open-circuit voltage V_{OC} is shown in Fig. 33.2.

33.2.2 Design of Cd-Based Solar Cells

Solar cells can be made from silicon (Si), III–V compounds such as GaAs, or II–VI compounds such as Zn-based and Cd-based compound semiconductors. Of these materials, CdTe is the most attractive because of a number of advantages. CdTe is a direct-band-gap material with a band gap of 1.54 eV at room temperature. This is very close to the theoretically calculated optimum value for solar cells. CdTe has a high absorption coefficient (above 10^5 cm^{-1} at a wavelength of 700 nm), so that approximately 90% of the incident light is absorbed by a layer thickness of only 2 μm (compared with around 10 μm for Si), cutting down the quantity of semiconductor required. Therefore, CdTe is one of the most promising photovoltaic materials available for use in low-cost high-efficiency solar cells.

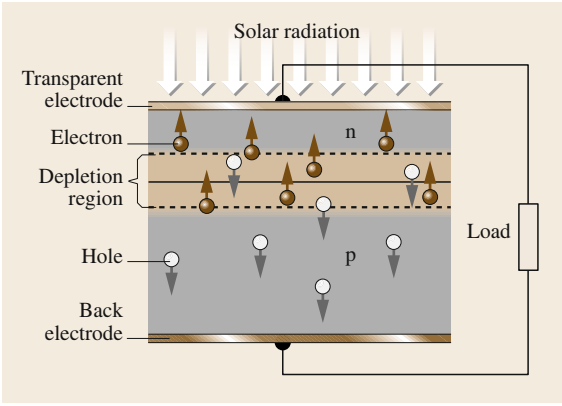

Fig. 33.1 The principle of photovoltaic devices

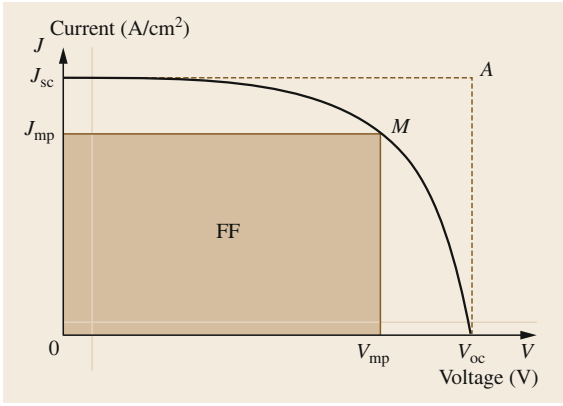

Fig. 33.2 Photovoltaic output characteristics of a solar cell

CdTe is the only material in which both n- and p-type conductivity can be easily controlled by doping acceptor or donor impurities in II–VI compound semiconductors. Furthermore, due to its high absorption coefficient and small carrier diffusion length, the junction must be formed closed to the surface, which reduces the carrier lifetime through surface recombination. In spite of this, the conversion efficiency has been gradually enhanced from 4% [33.2] to 16% [33.3] since the first CdTe-based solar cell was fabricated. CdTe solar cells can be made from polycrystalline or single-crystal material. However, it was found that this p–n homojuction structure is unstable due to the aging behavior of dopants in CdTe films and bulk single crystals [33.4]. Furthermore, it is also difficult to fabricate shallow p–n junctions with highly conducting surface layers, and high surface recombination velocities led to substantial losses that could not easily be avoided. For this reason, the CdS/CdTe heterojunction solar cell was proposed.

It has been proved that CdS/CdTe is a high-efficiency heterojunction solar cell. The theoretical calculation shows that this cell has a conversion efficiency of as high as 29% [33.5], and it is considered a promising alternative to the more widely used silicon devices. The typical structure of a CdS/CdTe solar cell is glass/indium tin oxide (ITO)/CdS/CdTe/back electrode, as seen in Fig. 33.3. The CdS/CdTe solar cell is based on the heterojunction formed between n-type CdS (only n-CdS is available) and p-type CdTe and is fabricated in a superstrate configuration where the incident light passes through the glass substrate, which has a thickness of 2−4 mm. This window glass is transparent, strong and cheap. This glass substrate also protects the active layers from the environment, and it provides the mechanical strength of the device. The outer face of the panel often has an antireflection coating to enhance absorption efficiency. A transparent conducting oxide (TCO) layer, usually tin oxide or indium tin oxide (ITO), acts as the front contact to the device. This is needed to reduce the series resistance of the device, which would otherwise arise from the thinness of the CdS layer. Usually, the polycrystalline n-type CdS layer is deposited onto the TCO. Due to its wide band gap ($E_g \approx 2.4$ eV at 300 K) it is transparent down to wavelengths of around 516 nm. The thickness of this layer is typically 100−300 nm. The CdTe layer is p-type-doped and its thickness is typically around 10 μm. Generally, the carrier concentration in CdS layer is 2–3 orders greater than that of the CdTe layer. As a result, the potential is applied mostly to the CdTe absorber layer, i. e., the depletion region is mostly within the CdTe layer. Therefore, the photogenerated carriers can be effectively separated in this active region.

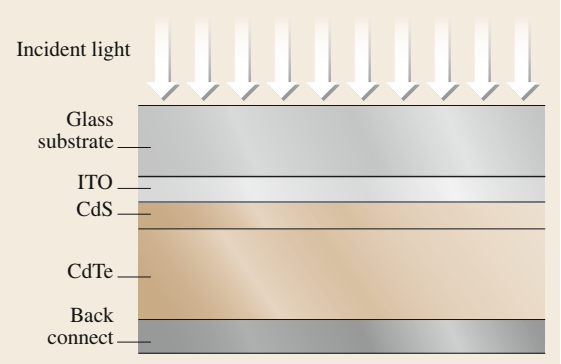

Fig. 33.3 A typical CdS/CdTe solar cell

The electrode preparation is very important in obtaining Ohmic contact or minimal series resistivity. Since there are no metals with a work function higher than the hole affinity of p-type CdTe (−5.78 eV) [33.6], it is difficult to produce a complete Ohmic contact on p-type CdTe surface. Many methods have been tried to fabricate Ohmic contact to p-type CdTe. Different metals or alloy and compounds such as Au, Al, and ZnTe/Cu etc. have also been used to serve as electrode materials. Although significant effort has been applied to this issue, the junction still inevitably displays some Schottky-diode characteristics. This is a problem that will be continuously studied.

33.2.3 Development of CdS/CdTe Solar Cells

The layers of CdS and CdTe for solar cells can be prepared using various techniques, which are summarized in Table 33.1. In these techniques, evaporation, close-space sublimation (CSS), screen printing and electrodeposition (ED) have been demonstrated to be very effective for fabricating high-efficiency large-area CdS/CdTe solar cells.

Study of solar cells based on CdTe single crystals and polycrystalline films were started as early as 1963 [33.14]. The cells were prepared with a p-type copper-telluride surface film as an integral part of the photovoltaic junction. The junction was thought to be a heterojunction between the p-type copper telluride and the n-type CdTe, with the transition region extending well into the CdTe side. A similar structure was reported for single-crystal cells. A conversion efficiency of up to 6% was obtained in the film cells, and 7.5% for single-crystal cells.

Dutton and *Muller* [33.15] fabricated CdS/CdTe solar cells by standard vapor-deposition procedures with a very thin CdTe layer. The existence of the

Table 33.1 Some fabrication techniques and conversion efficiency of CdS/CdTe solar cells

Fabrication techniques of CdS and CdTe	Conversion		Reference
	Efficiency (%)	Area (cm^2)	
Evaporation: physical vapor deposition (PVD), and chemical vapor deposition (CVD)	11.8	0.3	[33.7]
Close-spaced sublimation (CSS)	16	1.0	[33.3]
	8.4	7200	[33.8]
Electrodeposition (ED)	14.2	0.02	[33.9]
Screen printing (SP) and sintering	12.8	0.78	[33.10]
Metalorganic CVD (MOCVD)	11.9	0.08	[33.11]
PVD vacuum evaporation	11.8	0.3	[33.7]
Molecular beam epitaxy (MBE)	10.5	0.08	[33.12]
Sputtering deposition (SD)	14	0.09	[33.13]

interfacial layer was confirmed using x-ray diffraction studies, and substantiated by diode photocurrent measurements. The results showed a threshold photon energy that corresponds to the band gap of CdTe. The thin CdTe layer resulted in excellent rectification ratios and high reverse breakdown voltages. The observed photoresponse, *I–V* (current versus voltage), and *C–V* (capacitance versus voltage) characteristics were consistence with those predicted by a semiconductor heterojunction model of the CdS–CdTe interface. *Mitchell* et al. [33.16] prepared a variety of CdS/CdTe heterojunction solar cells with an ITO coating and a glycerol antireflection coating by vacuum evaporation of n-CdS films onto single-crystal p-CdTe substrates. Comparisons were made between cells prepared using different substrate resistivity, substrate surface preparations, and CdS film resistivity. The mechanisms of controlling the dark junction current, photocarrier collection, and photovoltaic properties were modeled, taking account of the interface states of the junction. A conversion efficiency of 7.9% was obtained under 85 mW/cm^2 of solar simulator illumination.

At the end of the 1970s, a new process, screen printing and sintering, was developed for fabricating CdS/CdTe polycrystal solar cells by *Matsushita* and coworkers [33.10, 17–20]. This technique proved to be a very effective method for fabricating large-area CdS/CdTe

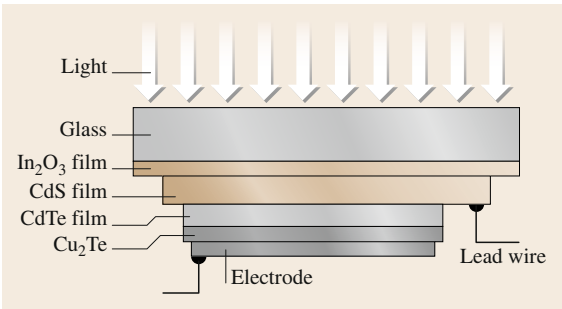

Fig. 33.4 Cross section of a ceramic thin-film CdTe solar cell

film solar cells. There are several important parameters in the screen-printing technique: the viscosity of the paste, the mesh number of the screen, the snap-off distance between the screen and the substrate and the pressure and speed of the squeegee. As cadmium chloride ($CdCl_2$) has a low melting point ($T_m = 568\,°C$), and forms a eutectic with both CdS and CdTe at low temperature, and the vapor pressure at 600 °C is high enough to allow complete volatilization of $CdCl_2$ after the sintering process, $CdCl_2$ is used as an ideal flux for sintering both CdS and CdTe.

Nakayama et al. [33.18] prepared the first thin-film CdS/CdTe solar cells using the screen-printing technique (Fig. 33.4). A glass plate, which was coated successively with In_2O_3 film and CdS ceramic thin film, was used as a transparent Ohmic contact substrate. The n-type CdS film with a thickness of about 20 μm and a resistivity of 0.2 Ω cm was prepared on this substrate by the screen-printing method. The CdTe paste was printed onto the CdS layer using the same technique and then heat-treated in an N_2 atmosphere at temperatures of 500–800 °C. As a result, the p-type CdTe layer with a thickness of 10 μm showed a resistivity of 0.1–1 Ω cm. A silver (Ag) paste electrode was applied to the p-type layer and an In–Ga alloy was applied to the CdS layer. The cell, with an active area of 0.36 cm^2, showed an intrinsic solar conversion efficiency of 8.1% under an illumination of 140 mW/cm^2 solar simulator (AM0). Subsequently, this group continued to work on improving CdS/CdTe solar cells [33.10, 19, 20]. From the practical point of view, a modular solar cell is necessary. For this purpose, thin-film CdS/CdTe solar cells with an efficiency of 6.3% were prepared on a borosilicate-glass substrate of $4 \times 4\,cm^2$ by successively screen printing and heating (sintering) of each paste of CdS, CdTe and carbon [33.19]. Although they fabricated some structures, including dividing the CdTe film on one substrate into five small cells, to prevent increases in the series resistivity, a 1 W module only showed an efficiency of 2.9% from 25 elemental cells with a $4 \times 4\,cm^2$ substrate. A main reason for this

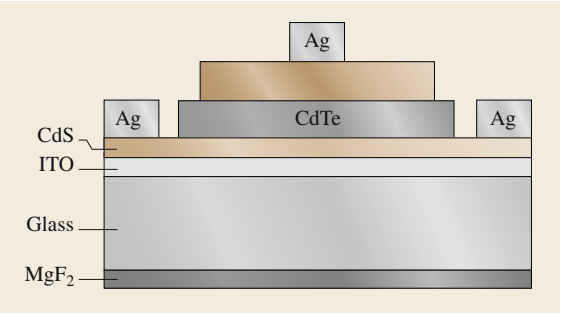

Fig. 33.5 The cross-sectional structure of a CdS/CdTe solar cell fabricating by the screen-printing method

low efficiency was thought to be the high series resistivity.

In order to decrease the resistivity of the carbon electrode further, this group changed the heating conditions of the carbon electrodes for CdTe and examined the effect of impurities in the carbon paste on the characteristics of solar cells [33.10]. They found that the series resistance (R_s) and the conversion efficiency (η) of solar cells exhibited strong dependence on the oxygen (O_2) partial pressure during the heating process. The results showed that the addition of Cu to the carbon paste causes R_s and the diode factor (n) to decrease, resulting in a remarkable improvement in η. Using a low-resistance contact electrode, which was made from 50 ppm added Cu carbon paste, a cell with an active area of 0.78 cm^2 displayed $V_{oc} = 0.754$ V, $I_{sc} = 0.022$ A, FF= 0.606 and $\eta = 12.8\%$.

Britt and *Ferekides* [33.21] reported the fabrication and characteristics of high-efficiency thin-film CdS/CdTe heterojunction solar cells. CdS films with 0.07–0.10 μm in thickness were deposited on a 0.5-μm SnO_2:F transparent conducting oxide layer by chemical-bath deposition and p-CdTe films with a thickness of 5 μm were deposited on the CdS layer by using the CSS method. Prior to the deposition of CdTe, CdS/SnO_2:F/glass was annealed in a H_2 atmosphere at temperatures of 350–425 °C for 5–20 min. The characteristics of the CdS/CdTe solar cell were $V_{oc} = 843$ mV, $J_{sc} = 25.1$ mA/cm^2, FF = 74.5%, corresponding to a total area greater than 1 cm^2 with an air mass 1.5 (AM1.5) conversion efficiency of 15.8%.

With modern growth techniques, high-efficiency CdS/CdTe solar cells have been developed using ultrathin CdS films having a thickness of 50 nm [33.3]. Figure 33.5 shows the cross-sectional structure of a CdS/CdTe solar cell. CdS films were deposited on an ITO glass substrates by the metal organic chemical vapor deposition (MOCVD) technique, and CdTe films were subsequently deposited by the CSS technique (see Fig. 33.6) for the fabrication of CdS/CdTe solar cells.

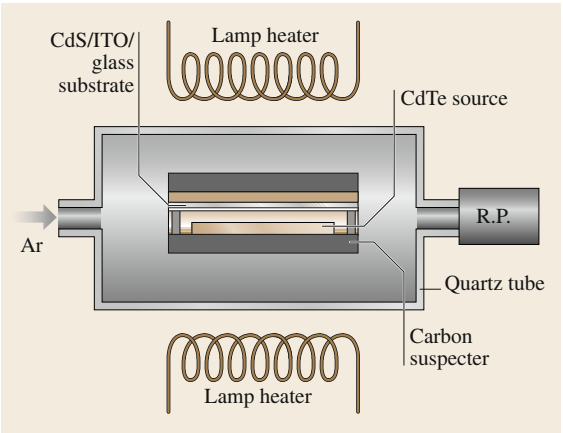

Fig. 33.6 Schematic of the close-spaced sublimation apparatus used for depositing CdTe films

A thin-film CdS/CdTe solar cell with an area of 1.0 cm^2 under AM1.5 conditions showed $V_{oc} = 840$ mV, $J_{sc} = 26.08$ mA/cm^2 and FF = 73%. As a result, a high conversion efficiency of 16.0% was achieved. Furthermore, they made developments in improving the uniformity of thickness and film qualities of CdS in order to obtain more efficient solar cells and to realize film deposition on large-area substrates of 30 × 60 cm or more [33.22]. They found clear differences in the electrical and optical properties between high- and low-quality CdS films. A photovoltaic conversion efficiency of 10.5% was achieved by a solar module with an area of 1376 cm^2 under AM1.5 measurement conditions.

In addition to dry processes such as screen printing, close-spaced sublimation etc., electrodeposition [33.23–26] has been also investigated for preparing polycrystalline CdTe layers for solar cells. *Awakura* and coworkers [33.24–26] reported the cathodic deposition behavior of CdTe thin layers under irradiation by visible light using ammoniacal basic aqueous solution as an electrolytic bath. Both deposition current density and current efficiency for the CdTe deposition were enhanced by irradiation. The deposited rate was over 10 times high than nonphotoassisted electrodeposition. This was believed to represent significant progress in reducing the cost of Cd-based solar cells.

To date, solar cells with an n-CdS/p-CdTe heterojunction have been reported with efficiencies as high as 16% [33.3]. Recently, it was reported that thin-layered n-CdS/p-CdTe heterojunction solar cells have already been manufactured industrially [33.27]. n-CdS film with a thickness range of 500–1000 Å was deposited from an aqueous solution directly onto a transparent conductive oxide (TCO) substrate. After the CdS film was annealed for densification and grain growing, p-CdTe layer was formed by electrochemical deposition.

The CdTe film was then annealed in air at 450 °C. Subsequently, monolithic TCO/CdS/CdTe was cut into discrete cells using an infrared laser. After other preparing process, a maximum efficiency of 10.6% for a CdTe 0.94 m^2 module with a power of 91.5 W was fabricated. The test results showed good stability. For practical applications, a 10-MW CdTe solar-cell manufacturing plant has been constructed [33.27].

33.2.4 CdZnTe Solar Cells

The ternary compound cadmium zinc telluride (CdZnTe, CZT) has potential for the preparation of high-efficiency tandem solar cell since its band gap can be tuned from 1.45 to 2.26 eV [33.28, 29]. *McCandless* et al. [33.28] deposited $Cd_{1-x}Zn_xTe$ films using the physical vapor deposition (PVD) and vapor transport deposition (VTD) techniques. The film composition was between 0.35 and 0.6, corresponding to a band gap from 1.7 to 1.9 eV. Post-deposition treatment of CdZnTe films in $ZnCl_2$ vapor at 400 °C resulted in no change to the alloy composition and caused recrystallization. Solar cells made from $Cd_{1-x}Zn_xTe$ films with $x \approx 0.35$ exhibited $V_{oc} = 0.78$ V and $J_{sc} < 10\,mA/cm^2$. These results were similar to those obtained from CdS window layers. Analysis of the spectral response indicated that $Cd_{1-x}Zn_xTe$ with $x \approx 0.35$ has a band gap of about 1.7 eV. *Gidiputti* et al. [33.29] used two deposition technologies, cosputtering from CdTe and ZnTe targets and coclose-spaced sublimation (CCSS) from CdTe and ZnTe powders, to prepare CdZnTe films. A structure similar to the CdTe superstrate configuration was initially utilized for cell fabrication: glass/ITO/CdS/CZT/graphite. Typical solar cell parameters obtained for CdZnTe/CdS (when $E_g(CdZnTe) = 1.72$ eV) solar cells were $V_{oc} = 720$ mV, and $J_{sc} = 2\,mA/cm^2$. However, the spectral response indicated increasing loss of photocurrent at longer wavelengths. In order to improve the collection efficiency, CdZnTe devices were annealed in a H_2 atmosphere. This postprocessing treatment showed that J_{sc} increased to over $10\,mA/cm^2$. Study of CdZnTe solar cells is being carried out in various directions.

33.2.5 The Future of Cd-Based Solar Cells

From the development process of Cd-based solar cells, the study on the laboratory scale is being transfered to large-scale deposition and cell fabrication. Modules are being developed throughout the world, using the screen printing, evaporative deposition and close-space sublimation [33.30–32]

In order to make a commercial Cd-based photovoltaic cell with its full potential, a large-scale high-throughput manufacturing process is required. The process must possess excellent yields and produce high-efficiency devices with good long-term stability. In order to progress towards these goals, a pilot system for continuous, inline processing of CdS/CdTe devices has been developed [33.33–35]. High-quality low-cost thin-film CdTe modules with an average total area efficiency of 8% and cascaded production-line yield of > 70% have been manufactured, and technology-development programs will further increase production-line module efficiency to 13% within five years [33.35].

33.3 Radiation Detectors

A radiation detector is a device that converts a radiation ray into electrical signal. They can be divided into gas-filled detectors, scintillation detectors and semiconductor detectors. Since semiconductor radiation detectors have a high spectrometric performance, and can be made portable, they have been applied in nuclear safeguards, medical physics and imaging diagnosis, industrial safety, nondestructive analysis, security and monitoring, nonproliferation and astrophysics [33.36, 37]. Meanwhile, they are also being gradually improved.

33.3.1 Basic Description of Semiconductor Radiation Detectors

The principle of operation of a semiconductor radiation detector is shown in Fig. 33.7. When high-energy photons (x- or γ-rays) radiate the detector, they lose the energy to induce electron–hole pairs in the semiconductor through photoelectric or Compton interactions, thereby increasing the conductivity of the material. In order to detect the change in conductivity, a bias voltage is required. An externally applied electric field separates the electron–hole pairs before they recombine, and electrons drift towards the anode, holes to the cathode. The charges are then collected by the electrodes. The collected charges produce a current pulse, whose integral equals the total charge generated by the incident photons, indicating the radiation intensity. The read-out goes through a charge-sensitive preamplifier, followed by a shaping amplifier. The multichannel analyzer is used for spectroscopic measurements of the radiation ray. This type of detector can produce both

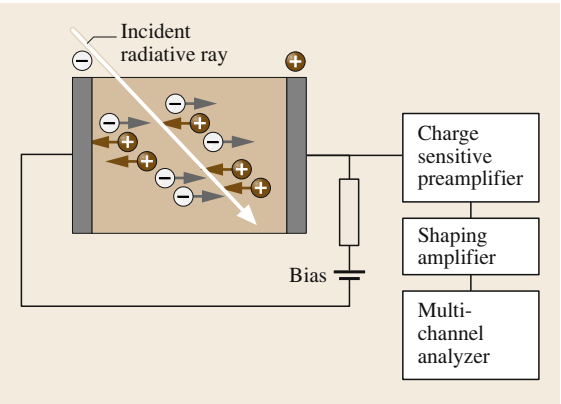

Fig. 33.7 The principle of operation of a semiconductor detector

count and energy information. Typically, detectors are manufactured in a square or rectangular configuration to maintain a uniform bias-current distribution throughout the active region. The wavelength of the peak response depends on the material's band-gap energy.

There are several important parameters to describe a detector performance. Detection efficiency is defined as the percentage of radiation incident on a detector system that is actually detected. Detector efficiency depends on the detector size and shape (larger areas and volumes are more sensitive), radiation type, material density (atomic number), and the depth of the detection medium. Energy resolution is one of the most important characteristics of semiconductor detectors. It is usually defined as the full-width at half-maximum (FWHM) of a single-energy peak at a specific energy. High resolution enables the system to more clearly resolve the peaks within a spectrum. So the reliability of the detector is also high. Detector sensitivity implies minimal detectable counts. It is defined as the number of counts that can be distinguished from the background. The relative detector response factor expresses the sensitivity of a detector relative to a standard substance. If the relative detector response factor is expressed on an equal-mass (-weight) basis, the determined sensitivity values can be substituted for the peak area.

33.3.2 CdTe and CdZnTe Radiation Detectors

Semiconductor radiation detectors are fabricated from a variety of materials including: germanium (Ge), silicon (Si), mercuric iodide (HgI_2), CdTe, CdZnTe etc. Typical detectors for a given application depend on several factors. Table 33.2 shows the features of some semiconductor detectors. From Table 33.2, Ge detectors have the best resolution, but require liquid-nitrogen cooling, which makes them impractical for portable applications. Si detectors also need cooling, and are inefficient in detecting photons with energies greater than a few tens of keV. CdTe and CdZnTe detectors possess their own advantages.

Single crystals of CdTe and CdZnTe are very important materials for the development of x- and γ-ray detectors. Currently Ge and Si detectors have to be used at liquid-nitrogen temperatures, and suffer from poor detection efficiency. Since the compound semiconductors CdTe and CdZnTe with high atomic number ($Z_{Cd} = 48, Z_{Zn} = 30, Z_{Te} = 52$) have a significantly higher photoelectric absorption efficiency in the $-100-500$ keV range, they can be fabricated into detectors that provide two advantages for use in portable instrumentation: (1) the large band-gap energy ($E_g > 1.54$ eV at room temperature) results in extremely small leakage current of a few nanoamps at room temperature. Therefore, these detectors have the potential to serve as useful detectors for radiation spectroscopy without the need for cryogenic cooling as required for more conventional silicon and hyper-pure germanium detectors; (2) the high density of the crystal provides excellent stopping power over a wide range of energies. The ability to operate at room temperature without the need for liquid-nitrogen cooling allows the construction of compact devices. CdTe and CdZnTe detectors can be fabricated into a variety of shapes and sizes, which makes it possible to produce detectors capable of meeting the requirements of a wide assortment of applications that are unsupported by other detector types. Their small size and relatively simple electronics allow them to open new areas of detector application. In many instances, CdTe and CdZnTe detectors can be substituted for other detector types in existing applications.

Table 33.2 The features of some semiconductor detectors

	NaI	Si	Ge	CdTe	$Cd_{0.9}Zn_{0.2}Te$
Bandgap (eV) at 300 K	–	1.14	0.67	1.54	1.58
Density (g/cm^3)	3.67	2.33	5.35	6.2	5.78
Energy per e–h pair (eV)	–	3.61	2.96	4.43	4.64
Detection/absorption	High	Low	Medium	High	High
Operation at room temp.	Yes	Yes	No	Yes	Yes
Spectrometic performance	Medium	High	Very high	High	High

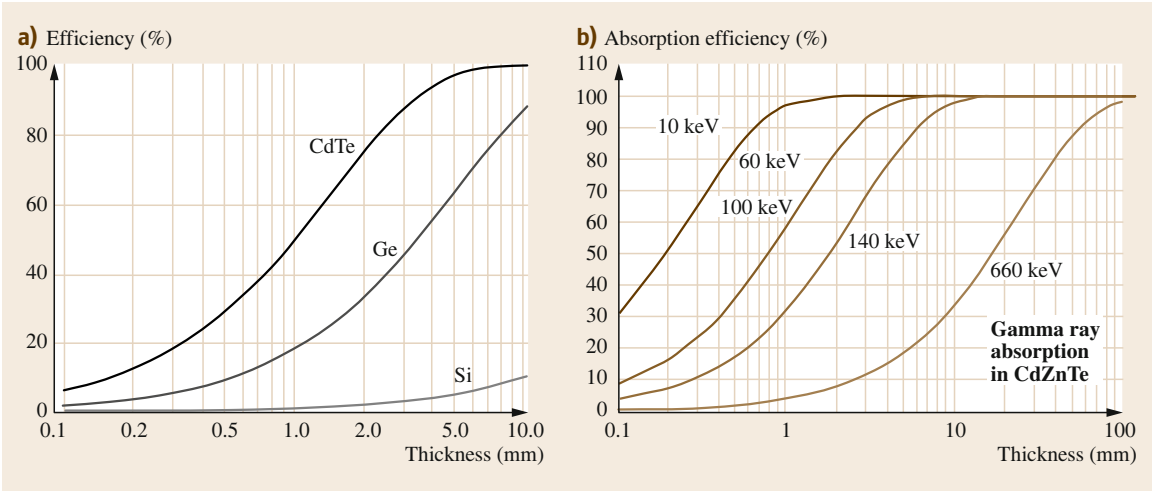

Fig. 33.8a,b γ-ray absorption in CdTe **(a)** and CdZnTe **(b)** detectors as a function of thickness

Figure 33.8 shows the γ-ray absorption efficiency in CdTe (Fig. 33.8a), and CdZnTe (Fig. 33.8b) detectors as a function of thickness. It was reported that, for a detector with a thickness of about 10 mm detecting 100 keV γ-rays, the detection efficiency for a CdTe detector is 100%, for a Ge detector 88%, for a Si detector only 12% [33.38]. In the case of a CdZnTe detector, CdZnTe with a thickness of only about 7 mm can absorb 100% of the γ-rays [33.39]. This efficiency assumes that the γ-ray is completely absorbed and the generated electron–hole pairs are completely collected. In fact, a large amount of charge loss occurs in CdTe and CdZnTe detector, depending on the quality of the materials.

33.3.3 Performance of CdTe and CdZnTe Detectors

Although CdTe and CdZnTe have many advantages over Si and Ge, including higher attenuation coefficients and lower leakage currents due to the wider bandgap, their disadvantages limit their application range [33.40]. The main disadvantage is that their crystals usually contain higher density defects. These defects are remaining impurities and structural defects such as mechanical cracks, twins, grain and tilt boundaries, and dislocations all lower the crystalline perfection of the materials.

In CdTe and CdZnTe detectors, the charge transport determines the collection efficiency of generated electron-hole pairs, and structural properties of materials control the uniformity of the charge transport. The problem of poor transport and collection of carriers, especially hole, can be overcome by applying high voltage to device and a range of electrode config. The former is related to high resistivity material, and later is related to the design of a detector. In addition, it was found that detected pulse signal intensity degraded with the time [33.41, 42]. This phenomenon was thought to be mainly related to the defects existing in bandgap. When the detector starts to work, these defects could act as slowly ionized acceptors. The low resistivity and poor quality material always exhibits such a polarization effect.

Summarizing above, improvement of a detector performance is equivalent to the improvement of the crystallinity of CdTe and CdZnTe. The key feature of all applications except substrate materials of CdTe and CdZnTe is the resistivity. This is because high resistivity can be obtained only by controlling native defects and impurity concentration. For many years, much effort was done in preparing high quality CdTe and CnZnTe single crystals.

Progresses in Crystal Growth of High Quality CdTe and CdZnTe

Various techniques have been applied to grow high-quality CdTe and CdZnTe single crystals. The Bridgman method [33.43, 44], the traveling-heater method [33.45, 46], growth from Te solvent [33.47], the gradient-freeze method [33.48, 49], and physical vapor transport [33.50, 51] are the most widely used. Crystals with applicable quality and size have become available, and have also fostered the rapid progress of research on CdTe.

As-grown CdTe single crystals commonly contain high concentration of both residual impurities and intrinsic defects. Preparation of high-purity high-resistivity CdTe and CdZnTe crystals has been widely attempted [33.52]. Early works was done by *Triboulet*

and *Marfaing* [33.53] in obtaining high-purity lightly compensated zone-melting growth following synthesis by the Bridgman method. The room-temperature carrier concentrations range from $1-5\times10^{13}\,\mathrm{cm}^{-3}$, and the resistivity from 100 to 400 Ω cm. The carrier mobility at 32 K reaches as high as $1.46\times10^{5}\,\mathrm{cm}^{2}/(\mathrm{V\,s})$. The total concentration of electrically active centers was estimated to be about $10^{14}\,\mathrm{cm}^{-3}$.

Usually, as-grown CdTe crystal shows p-type conductivity owing to the existence of remaining acceptor impurities or native defects. For this reason, many results have been reported in preparing high-resistivity CdTe. Chlorine (Cl) is thought to be a suitable donor for the compensation of these remaining acceptors because Cl can be doped quite uniformly due to its very small segregation coefficient [33.54].

The growth of high-resistivity CdTe:Cl single crystals with device quality was successfully performed by the traveling-heater method (THM) [33.54]. Solvent alloys for THM growth were synthesized in ampoules filled with Te, CdTe and $CdCl_2$ so that the molar ratio of Te/Cd was the same as in the solvent zone during the growth. The Cl concentration in the grown crystal was 2 weight-ppm. According to the dynamics of the crystal growth, it is important to control the shape of the solid–liquid to grow high-quality single crystals. Therefore, the solvent volume was optimized. The use of a slightly tilted seed from ⟨111⟩B was also effective in limiting the generation of twins with different directions. Single-crystal (111) wafers, larger than $30\times30\,\mathrm{mm}^2$ were successfully obtained from a grown crystal with a diameter of 50 mm. Pt/CdTe/In detectors with dimensions of $2\times2\times0.5\,\mathrm{mm}^3$ showed better energy resolution, because a higher electric field can be applied. The effective detector resistivity was estimated to be 10^{11} Ω cm.

CdTe doped with chlorine (Cl) or indium (In) with a resistivity of 3×10^{9} Ω cm and CdZnTe with a resistivity of 5×10^{10} Ω cm were grown by the high-pressure Bridgman (HPB) technique [33.55]. The material was polycrystalline with large grains and twins. Although the crystalline quality of HPB CdTe and CdZnTe is poor, the grains are large enough to obtain volume detectors of several cm^3. Photoluminescence (PL) spectra at 4 K showed that the free exciton could be observed and the FWHM of the bound excitons is very low. Some impurity emissions were identified. The detectors were fabricated from HPB CdTe and CdZnTe. These detectors showed excellent performance. Gamma-ray spectra were presented with high-energy resolution in an energy range from 60 to 600 keV. Using a $10\times10\times2\,\mathrm{mm}^3$ HPB detector, at a bias of 300 V, the peak at 122 keV from ^{57}Co had a FWHM of 5.2 KeV. Detectors with high-energy resolution were fabricated.

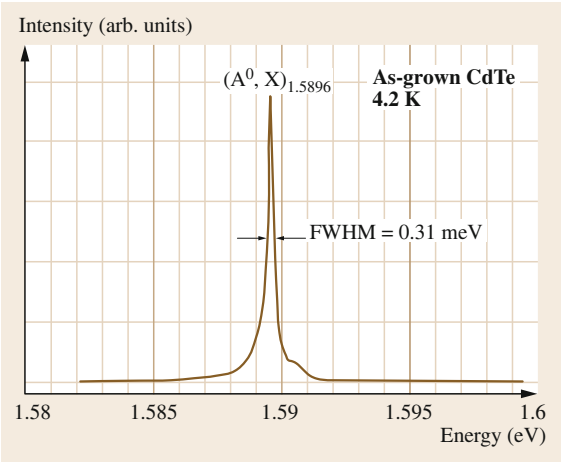

Fig. 33.9 A typical high-resolution PL spectrum of a high-purity CdTe sample

Because of the difference in vapor pressure between Cd and Te, grown crystals contain a large number of Cd vacancies (V_{Cd}). These Cd vacancies manifest acceptor behaviour. Therefore, high-resistivity CdTe can also be obtained by controlling the concentration of Cd vacancies. However, a prerequisite is that the purity of the CdTe crystal is high enough that the remaining impurities do not play a substantial role in determining the conductivity. Recently, the preparation of ultra-high-purity CdTe single crystals was reported [33.56, 57]. In order to obtain a high purity the starting materials of Cd and Te, Cd were first purified by vacuum distillation (VD) and the overlap zone-melting (OZM) method [33.56], while Te was purified using the normal freezing method [33.57]. The results of glow-discharge mass spectroscopy (GDMS) and the measurement of the residual resistivity ratio (RRR) showed that refined Cd and Te had the purity of 6N-up. Using the refined Cd and Te as starting materials, extremely high-purity twin-free CdTe single crystals were prepared by the traditional vertical Bridgman technique. Figure 33.9 shows a typical high-resolution PL spectrum of a high-purity CdTe sample. Only a sharp and strong emission line of (A^0, X) (an exciton bound to a neutral acceptor) at 1.5896 eV was observed. The FWHM of the (A^0, X) line is 0.31 meV. This is the narrowest value ever reported for CdTe single crystals grown by the Bridgman method. All of the above indicate that the sample is of high purity and quality. For a good performance detector, the leakage current must not exceed a few nanoamps, which requires a material with high resistivity. When growing CdTe crystals, the CdTe contain large number of Cd vacancies due to the extreme volatility of Cd. For these reason, CdTe single crystals were annealed in a Cd atmosphere in order to

obtain a high-resistivity crystal. Hall-measurement results showed that the conductive type changed from as-grown p-type to n-type at a Cd pressure around 1.5×10^{-2} atm, corresponding to a Cd source temperature of 500 °C. Samples annealed under these conditions showed a resistivity as high as $10^9\ \Omega$ cm.

Lachish [33.58] grew CdTe and CdZnTe crystals with excess cadmium in order to avoid the Te precipitates found in crystals grown by Bridgman method. During crystal growth one ampoule end was kept at a low temperature, which determines a constant, nearly atmospheric, vapor pressure in the system. The constant vapor pressure maintains a constant liquid composition and balanced amounts of cadmium and tellurium within the crystal. Although the highly donor-doped crystals are highly electrically conducting, successive annealing in Te vapor transforms the crystal wafers into a highly compensated state showing high electrical resistivity and high gamma sensitivity, depending on the doping level.

Improvements of Transport and Collection of Carriers in CdTe and CdZnTe Detectors

The transport and collection of carriers in CdTe and CdZnTe, especially holes, are the main problems that affect their performance. Poor carriers transport causes position-dependent charge collection and limits their capability as high-resolution spectrometers [33.59]. As a result, this limits the volume of detector. Therefore, the efficient detecting resolution and range are decreased. *Amman* et al. [33.60] studied the affect of nonuniform electron trapping on the performance of a γ-ray detector. An analysis of the induced charge signals indicated that regions of enhanced electron trapping are associated with inclusions, and that these regions extend beyond the physical size of the inclusions. Such regions introduce nonuniform electron trapping in the material that then degrades the spectroscopic performance of the material as a γ-ray detector. The measurements showed that the degree of nonuniformity that affects detector performance could be at the 1% level. Consequently, any useful characterization and analysis technique must be sensitive down to this level.

Detectors equipped with Ohmic contacts, and a grounded guard ring around the positive contact, have a fast charge-collection time. Conductivity adjustment, in detectors insensitive to hole trapping, optimizes the detector operation by a trade-off between electron lifetime and electrical resistance. Better hole collection has been achieved by designing detectors and electrodes of various geometries. *Nakazawa* et al. [33.61] improved the CdTe diode detectors by fabricating the guard-ring structure in the cathode face, and the leakage current of the detector decreased by more than an order of magnitude. The new CdTe detector was operated with a bias as high as 800 V at 20 °C and showed a good energy resolution (0.93 keV and 1 keV FWHM for 59.5 keV and 122 keV, respectively) and high stability for long-term operation at room temperature. Furthermore, they also developed a large-area ($20 \times 20\ \text{mm}^2$) detector with very high resolution. Owing to its high stopping power and high resolution at room temperature, pixel imagers have also been developed in the same group, and it is thought that this large diode detector could possibly be a substitute for scintillation detectors.

Since the carriers drift slow and have a short lifetime in CdTe detectors, the number of photons in the photo-peak is reduced and the spectrum is distorted by a tail towards lower energies. For these reasons, CdTe detectors are usually made into Schottky diodes, because this structure can withstand much higher bias voltage with a leakage current orders of magnitude lower than detectors with Ohmic contacts. *Takahashi* et al. [33.62] adopted the configuration of Schottky CdTe diode, which due to the low leaking current, makes it possible to apply a much higher bias voltage to ensure complete charge collection in relatively thin (< 1 mm) devices. Both the improved charge-collection efficiency and the low leakage current lead to an energy resolution of better than 600 eV FWHM at 60 keV for a $2 \times 2\ \text{mm}^2$ device without any electronics for charge-loss correction. Meanwhile, they also fabricated large-area detectors with dimensions of $21.5 \times 21.5\ \text{mm}^2$, with a thickness of 0.5 mm and an energy resolution of 2.8 keV. Stacked detectors can measure the energies as high as 300 keV. Furthermore, a large-array detector, consisting of 1024 individual CdTe diodes, was also made. Every detector had a dimension of $1.2 \times 5.0\ \text{mm}^2$. The total area, including the spaces between the detector elements, is $44 \times 44\ \text{mm}^2$. This array detector is expected to be used in next-generation Compton telescopes.

33.3.4 Applications of CdTe and CdZnTe Detectors

Owing to the convenience of the smaller collimator, better resolution and temperature stability, CdTe and CZT detectors have been used in safeguard applications by the International Atomic Energy Agency (IAEA) and some countries for over ten years [33.63, 64]. With the gradual improvement in performance, CdTe and CdZnTe detectors are replacing NaI detectors used in spent-fuel attribute tests [33.65], though their sensitivity is still low compared to NaI and Ge detectors, although already sufficient for many applications. CdTe detectors have a sensitive volume of

about 20–100 mm^3 and a probe diameter of 8–9 mm. CdZnTe detectors have a larger volume than CdTe detectors. The largest commercial CdZnTe detectors have a geometric volume of 1687 mm^3 ($15 \times 15 \times 7.5\ mm^3$). Detectors are mainly of hemispheric design to obtain high carrier-collection efficiency. These large-volume detectors have been made into portable and hand-held isotope-identification devices and are being used to detect radioactive sources.They will become commercially available in the near future.

At present, conventional x-ray film or scintillator mammograms are used in medical diagnostics such as screening for breast cancer. However, these show a nonlinear response to x-ray intensity and the detection quantum efficiency is low. Room-temperature semiconductor detectors such as CdTe and CdZnTe have favorable physical characteristics for medical applications. From the start of these investigations in the 1980s, rapid progress has been achieved [33.66–71]. *Barber* [33.67] presented results concerning, first, a CdTe two-dimensional (2-D) imaging system ($20 \times 30\ mm^2$ with 400×600 pixels) for dental radiology and, second, a CdZnTe fast pulse-correction method applied to a $5 \times 5 \times 5\ mm^3$ CdZnTe detector (energy resolution of 5% for a detection efficiency of 85% at 122 keV) for medical imaging. After that, a 2 mm-thick CdZnTe detector was fabricated for application to digital mammography [33.69]. The preliminary images showed high spatial resolution and efficiency. Furthermore, CdTe and CdZnTe detectors with a thickness of 0.15–0.2 mm were fabricated [33.71]. The detectors are indium-bump-bonded onto a small version of a chip. Their detection quantum efficiency was measured as 65%. This result showed that CdTe and CdZnTe detectors are superior to scintillator-based digital systems, whose quantum efficiency is typically around 30–40%. This showed that CdTe and CdZnTe detectors have potential applications in medical imaging, as well as industrially for nondestructive evaluation inspection.

In universe exploration, Cd-based detectors can be used in an advanced Compton telescope (ACT) planned as the next-generation space-based instrument devoted to observations of low/medium-energy γ-rays ($\approx$ 0.2–30 MeV) and to the nonthermal energy exploration telescope (NeXT) [33.72]. In the universe, radiation rays have a wide energy range of 0.5–80 keV. In order to detect this wide range of radiation, *Takahashi* et al. [33.73–75] proposed a new focal-plane detector based on the idea of combining an x-ray charge-coupled device (CCD) and a CdTe pixel detector as the wide-band x-ray imager (WXI). The WXI consists of a soft-x-ray imager and a hard-x-ray imager. For the detection of soft x-rays (10–20 keV) with high positional resolution, a CCD with a very thin dead layer will be used. For hard x-rays, CdTe pixel detectors serve as absorbers. This study is now under way.

33.4 Conclusions

Devices fabricated from Cd-based compounds, such as solar cells and radiation detectors, are being applied in our daily life. In the case of solar cells, although recent success have improved their conversion efficiency and reduced the cost, many problems remain. Fundamental understanding of the CdTe-based solar-cell properties is limited, particularly as a result of their polycrystalline nature. Therefore, the fundamental electronic properties of polycrystalline Cd-based thin films should be studied deeply. Other challenges are to reduce the cost and to lengthen the operating life span. These problems are being studied and solved [33.76].

In the case of radiation detectors, CdTe and CdZnTe detectors have many advantages, such as room-temperature operation, high count rates, small size, and direct conversion of photons to charge, which make them attractive candidates for a wide variety of applications in industrial gauging and analysis, as well as medical instrumentation and other areas. These detectors are being made available commercially at present. However, they have severe problems such as polarization effects, long-term stability and their high price. Further efforts should still be focused on the preparation of high-quality materials and improvement of the stability and reliability of detectors. We are confident that radiation detectors made from Cd-based compounds will achieve more widespread application.

References

33.1 E. Becquerel: Compt. Rend. Acad. Sci. (Paris) **9**, 561 (1839)

33.2 Y.A. Vodakov, G.A. Lomakina, G.P. Naumov, Y.P. Maslakovets: Sov. Phys. Solid State **2**, 1 (1960)

33.3 T. Aramoto, S. Kumazawa, H. Higuchi, T. Arita, S. Shibutani, T. Nishio, J. Nakajima, M. Tsuji, A. Hanafusa, T. Hibino, K. Omura, H. Ohyama, M. Murozono: Jpn. J. Appl. Phys. **36**, 6304 (1997)

33.4 B. Yang, Y. Ishikikawa, T. Miki, Y. Doumae, M. Ishiki: J. Cryst. Growth **179**, 410 (1997)
33.5 A.W. Brinkman: Properties of narrow gap cadmium-based compounds. In: *Electronic Materials Information Services*, Vol. 10, ed. by P. Capper (IEE, London 1994) p. 591
33.6 R.W. Swank: Phys. Rev. **156**, 844 (1967)
33.7 R.G. Little, M.J. Nowlan: Progr. Photovolt. **5**, 309 (1997)
33.8 Y.-S. Tyan, E.A. Perez-Albuerne: Proc. 16th IEEE Photovolt. Specialists Conf. (IEEE, New York 1982) p. 794
33.9 J.M. Woodcock, A.K. Turner, M.E. Özsan, J.G. Summers: Proc. 22nd IEEE Photovolt. Specialists Conf., Las Vegas (IEEE, New York 1991) p. 842
33.10 K. Kuribayashi, H. Matsumoto, H. Uda, Y. Komatsu, A. Nakano, S. Ikegami: Jpn. J. Appl. Phys. **22**, 1828 (1993)
33.11 J. Britt, C. Ferekides: Appl. Phys. Lett. **62**, 2851 (1993)
33.12 H.W. Schock, A. Shah: Proc. 14th Eur. Photovolt. Sol. Energy Conf., ed. by H.A. Ossenbrink, P. Helm, H. Ehmann (H.S. Stephens, Bedford 1997) p. 2000
33.13 A.D. Compaan, A. Gupta, J. Drayton, S.-H. Lee, S. Wang: Phys. Stat. Solid B **241**, 779 (2004)
33.14 D.A. Cusano: Solid State Electron. **6**, 217 (1963)
33.15 R.W. Dutton, R.S. Muller: Solid State Electron. **11**, 749 (1968)
33.16 K.W. Mitchell, A.L. Fahrenbruch, R.W. Bube: J. Appl. Phys. **48**, 4365 (1977)
33.17 H. Uda, A. Nakano, K. Kuribayashi, Y. Komatsu, H. Matsumoto, S. Ikegami: Jpn. J. Appl. Phys. **22**, 1822 (1983)
33.18 N. Nakayama, H. Matsumoto, K. Yamaguchi, S. Ikegami, Y. Hioki: Jpn. J. Appl. Phys. **15**, 2281 (1976)
33.19 S. Ikegami, T. Yamashita: J. Electron. Mater. **8**, 705 (1979)
33.20 N. Nakayama, H. Matsumoto, A. Nakano, S. Ikegami, H. Uda, T. Yamashita: Jpn. J. Appl. Phys. **19**, 703 (1980)
33.21 J. Britt, C. Ferikides: Appl. Phys. Lett. **62**, 2851 (1993)
33.22 M. Tsuji, T. Aramoto, H. Ohyama, T. Hibino, K. Omura: Jpn. J. Appl. Phys. **39**, 3902 (2000)
33.23 M.P.R. Panicker, M. Knaster, F.A. Kröger: J. Electrochem. Soc. **125**, 566 (1978)
33.24 K. Murase, H. Uchida, T. Hirato, Y. Awakura: J. Electrochem. Soc. **146**, 531 (1999)
33.25 K. Murase, M. Matsui, M. Miyake, T. Hirato, Y. Awakura: J. Electrochem. Soc. **150**, 44 (2003)
33.26 M. Miyake, K. Murase, H. Inui, T. Hirato, Y. Awakura: J. Electrochem. Soc. **151**, 168 (2004)
33.27 D.W. Cunningham, M. Rubcich, D. Skinner: Prog. Photovolt. **10**, 59 (2002)
33.28 B. McCandless, K. Dobson, S. Hegedus, P. Paulson: Proc. NCPV Sol. Program Rev. Meet., Denver (NREL, Golden 2003) p. 401, NREL/CD-520-33586
33.29 G. Gidiputti, P. Mahawela, M. Ramalingan, G. Sivaraman, S. Subramanian, C.S. Ferekides, D.L. Morel: Proc. NCPV Sol. Program Rev. Meet., Denver (NREL, Golden 2003) p. 896, NREL/CD-520-33586
33.30 P.D. Maycock: PV News **17**, 3 (1998)
33.31 R.C. Powell, U. Jayamaha, G.L. Dorer, H. McMaster: Proc. NCPV Photovolt. Program, Rev., ed. by M. Al-Jassim, J.P. Thornton, J.M. Gee (American Institute of Physics, New York 1995) p. 1456
33.32 D. Bonnet, H. Richter, K.-H. Jager: Proc. 13th Eur. Photovolt. Sol. Energy Conf., ed. by W. Freiesleben, W. Palz, H.A. Ossenbrink, P. Helm (Stephens, Bedford 1996) p. 1456
33.33 K. Zweibel, H. Ullal: Proc. 25th IEEE Photovolt. Specialists Conf., Washington DC 1996 (IEEE, New York 1996) p. 745
33.34 K.L. Barth, R.A. Enzenroth, W.S. Sampath: Proc. NCPV Sol. Program Rev. Meet., Denver (NREL, Golden 2003) p. 904, NREL/CD-520-33586
33.35 A. Abken, C. Hambro, P. Meyers, R. Powell, S. Zafar: Proc NCPV Sol. Program Rev. Meet., Denver (NREL, Golden 2003) p. 393, NREL/CD-520-33586
33.36 K. Zanio: In: *Semiconductors and Semimetals*, Vol. 13, ed. by R.K. Willardson, A.C. Beer (Academic, New York 1978) p. 164
33.37 R. Triboulet, Y. Marfaing, A. Cornet, P. Siffert: J. Appl. Phys. **45**, 2759 (1974)
33.38 G. Sato, T. Takahashi, M. Sugiho, M. Kouda, T. Mitani, K. Nakazawa, Y. Okada, S. Watanabe: IEEE Trans. Nucl. Sci. **48**, 950 (2001)
33.39 C. Szeles: Phys. Stat. Solid B **241**, 783 (2004)
33.40 H. Yoon, J.M. Van Scyoc, T.S. Gilbert, M.S. Goorsky, B.A. Brunett, J.C. Lund, H. Hermon, M. Schieber, R.B. James: Proc. Infrared Appl. Semicond. II. Symp. Boston, ed. by D.L. McDaniel Jr., M.O. Manasreh, R.H. Miles, S. Sivananthan, P.A. Warrendale (Materials Research Society, Pittsburgh 1998) p. 241
33.41 R.O. Bell, G. Entine, H.B. Serreze: Nucl. Instrum. Methods **117**, 267 (1974)
33.42 P. Siffert, J. Berger, C. Scharager, A. Cornet, R. Stuck, R.O. Bell, H.B. Serreze, F.V. Wald: IEEE Trans. Nucl. Sci. **23**, 159 (1976)
33.43 R.K. Route, M. Woff, R.S. Feigelson: J. Cryst. Growth **70**, 379 (1984)
33.44 K.Y. Lay, D. Nichols, S. McDevitt, B.E. Dean, C.J. Johnson: J. Cryst. Growth **86**, 118 (1989)
33.45 R.O. Bell, N. Hemmat, F. Wald: Phys. Stat. Solid A **1**, 375 (1970)
33.46 R. Triboulet, Y. Mafaing, A. Cornet, P. Siffert: J. Appl. Phys. **45**, 375 (1970)
33.47 K. Zanio: J. Electron. Mat. **3**, 327 (1974)
33.48 M. Azoulay, A. Raizman, G. Gafni, M. Roth: J. Cryst. Growth **101**, 256 (1990)
33.49 A. Tanaka, Y. Masa, S. Seto, T. Kawasaki: Mater. Res. Soc. Symp. Proc. **90**, 111 (1987)
33.50 W. Akutagawa, K. Zanio: J. Cryst. Growth **11**, 191 (1971)
33.51 C. Ceibel, H. Maier, R. Schmitt: J. Cryst. Growth **86**, 386 (1988)
33.52 M. Isshiki: *Wide-Gap II–VI Compounds for Opto-Electronic Applications* (Chapman Hall, London 1992) p. 3
33.53 R. Triboulet, Y. Mafaing: J. Electrochem. Soc. **120**, 1260 (1973)
33.54 M. Funaki, T. Ozaki, K. Satoh, R. Ohno: Nucl. Instrum. Methods A **322**, 120 (1999)

33.55 M. Fiederle, T. Feltgen, J. Meinhardt, M. Rogalla, K.W. Benz: J. Cryst. Growth **197**, 635 (1999)
33.56 B. Yang, Y. Ishikawa, Y. Doumae, T. Miki, T. Ohyama, M. Isshiki: J. Cryst. Growth **172**, 370 (1997)
33.57 S.H. Song, J. Wang, M. Isshiki: J. Cryst. Growth **236**, 165 (2002)
33.58 U. Lachish: CdTe *and* CdZnTe *Crystal Growth and Production of Gamma Radiation Detectors*, http://urila.tripod.com/crystal.htm
33.59 T. Takahashi, S. Watanabe: IEEE Trans. Nucl. Sci. **48**, 950 (2001)
33.60 M. Amman, J.S. Lee, P.N. Luke: J. Appl. Phys. **92**, 3198 (2002)
33.61 K. Nakazawa, K. Oonuki, T. Tanaka, Y. Kobayashi, K. Tamura, T. Mitani, G. Sato, S. Watanabe, T. Takahashi, R. Ohno, A. Kitajima, Y. Kuroda, M. Onishi: IEEE Trans. Nucl. Sci. **51**, 1881 (2004)
33.62 T. Takahashi, T. Mitani, Y. Kobayashi, M. Kouda, G. Sato, S. Watanabe, K. Nakazawa, Y. Okada, M. Funaki, R. Ohno, K. Mori: IEEE Trans. Nucl. Sci. **49**, 1297 (2002)
33.63 R. Arlt, D.E. Rundquist: Nucl. Instrum. Methods Phys. Res. A **380**, 455 (1996)
33.64 T. Prettyman: Proc. 2nd Workshop Sci. Mod. Technol. Safeguards, Albuquerque, ed. by C. Foggi, E. Petraglia (European Commission, Albuquerque 1998)
33.65 W.K. Yoon, Y.G. Lee, H.R. Cha, W.W. Na, S.S. Park: INMM J. Nucl. Mat. Manag. **27**, 19 (1999)
33.66 C. Scheiber, J. Chambron: Nucl. Instrum. Methods A **322**, 604 (1992)
33.67 H.B. Barber: J. Electron. Mater. **25**, 1232 (1996)
33.68 L. Verger, J.P. Bonnefoy, F. Glasser, P. Ouvrier-Buffet: J. Electron. Mater. **26**, 738 (1997)
33.69 S. Yin, T.O. Tümay, D. Maeding, J. Mainprize, G. Mawdsley, M.J. Yaffe, W.J. Hamilton: IEEE Trans. Nucl. Sci. **46**, 2093 (1999)
33.70 C. Scheiber: Nucl. Instrum. Methods A **448**, 513 (2000)
33.71 S. Yin, T.O. Tümay, D. Maeding, J. Mainprize, G. Mawdsley, M.J. Yaffe, E.E. Gordon, W.J. Hamilton: IEEE Trans. Nucl. Sci. **49**, 176 (2002)
33.72 T. Tanaka, T. Kobayashi, T. Mitani, K. Nakazawa, K. Oonuki, G. Sato, T. Takahashi, S. Watanabe: New Astron. Rev. **48**, 269 (2004)
33.73 T. Takahashi, B. Paul, K. Hirose, C. Matsumoto, R. Ohno, T. Ozaki, K. Mori, Y. Tomita: Nucl. Instr. Meth. A **436**, 111 (2000)
33.74 T. Takahashi, K. Nakazawa, T. Kamae, H. Tajima, Y. Fukazawa, M. Nomachi, M. Kokubun: SPI **4851**, 1228 (2002)
33.75 T. Takahashi, K. Makishima, Y. Fukazawa, M. Kokubun, K. Nakazawa, M. Nomachi, H. Tajima, M. Tashiro, Y. Terada: New Astron. Rev. **48**, 309 (2004)
33.76 V.K. Krishna, V. Dutta: J. Appl. Phys. **96**, 3962 (2004)